A Section 508–conformant HTML version of this article is available at https://doi.org/10.1289/EHP4538.

Use of a Mouse Model and Human Umbilical Vein Endothelial Cells to Investigate the Effect of Arsenic Exposure on Vascular Endothelial Function and the Associated Role of Calpains

Zhihui Cai,[1] Yanqing Zhang,[1] Yutian Zhang,[1] Xiaofeng Miao,[1] Shu Li,[1] Hui Yang,[1] Qinjie Ling,[1] Peter R. Hoffmann,[2] and Zhi Huang[1]

[1]Department of Biotechnology, Jinan University, Guangzhou, Guangdong Province, China
[2]Department of Cell and Molecular Biology, John A. Burns School of Medicine, University of Hawaii, Honolulu, Hawaii, USA

Background: Arsenic (As) is a well-known environmental contaminant. Chronic exposure to As is known to increase the risk of cardiovascular diseases, including atherosclerosis, hypertension, diabetes, and stroke. However, the detailed mechanisms by which As causes vascular dysfunction involving endothelial integrity and permeability is unclear.

Objectives: Our goal was to investigate how exposure to As leads to endothelial dysfunction.

Methods: Arsenic trioxide (ATO) was used to investigate the effects and mechanisms by which exposure to As leads to endothelial dysfunction using a mouse model and cultured endothelial cell monolayers.

Results: Compared with the controls, mice exposed chronically to As (10 ppb in drinking water supplied by ATO) exhibited greater vascular permeability to Evans blue dye and fluorescein isothiocyanate–labeled bovine serum albumin (FITC-BSA). In addition, endothelial monolayers treated with ATO (0.13 μM As) exhibited greater intracellular gaps and permeability to low-density lipoprotein or transmigrating THP-1 cells. Furthermore, activity and protein levels of calpain-1 (CAPN-1) were significantly higher in aortas and human umbilical vein endothelial cells (HUVECs) treated with ATO. These results were consistent with effects of ATO treatment and included a rapid increase of intracellular calcium ($[Ca^{2+}]i$) and higher levels of CAPN-1 in the plasma membrane. Endothelial cell dysfunction and the proteolytic disorganization of vascular endothelial cadherin (VE-cadherin) in HUVECs in response to ATO were partially mitigated by treatment with a CAPN-1 inhibitor (ALLM) but not a CAPN-2 inhibitor (Z-LLY-FMK).

Conclusions: This study found that in mice and HUVEC models, exposure to ATO led to CAPN-1 activation by increasing $[Ca^{2+}]i$ and CAPN-1 translocation to the plasma membrane. The study also suggested that inhibitor treatment may have a role in preventing the vascular endothelial dysfunction associated with As exposure. The findings presented herein suggest that As-induced endothelial dysfunction involves the hyperactivation of the CAPN proteolytic system. https://doi.org/10.1289/EHP4538

Introduction

Arsenic (As) contamination is a well-known environmental problem (Jomova et al. 2011), which can lead to severe health disorders such as skin lesions, cardiovascular disease, liver toxicity, and multiple types of tumors (Naujokas et al. 2013). Although As exists ubiquitously in four possible oxidation states (−3, 0, +3 and +5) in the environment, trivalent arsenite [As(III)] and pentavalent arsenate [As(V)] are the predominant inorganic arsenic (iAs) species in natural water (Smedley and Kinniburgh 2002), whereas arsenite is more prevalent in groundwater (Korte and Fernando 1991). Chronic As exposure currently affects over 140 million people in at least 70 countries worldwide (Peters et al. 2015). In Asia, at least 60 million people were at risk of chronic As exposure, and more than 20 million people in China were estimated to be living in areas with As levels in the drinking water >10 μg/L (10 ppb), which is the World Health Organization (WHO) guideline value and the current Chinese standard for safe drinking water (Rodríguez-Lado et al. 2013). A cohort study (Moon et al. 2013) showed that long-term As exposure at low-to-moderate levels positively correlated with atherosclerosis. Accumulating evidence for endothelial toxicity by As exposure has been established, including inhibition of cell differentiation and induction of cell stress and apoptosis (Miller et al. 2002; Roboz et al. 2000). However, the molecular mechanisms by which As might lead to endothelial dysfunction have remained unclear.

Vascular endothelial cells tightly lining the inner face of vessel walls form a continuous monolayer that regulates vascular functions such as transport of molecules, trafficking of leukocytes, and angiogenesis (Bazzoni and Dejana 2004). Endothelial homeostasis is impacted by a wide variety of factors and changes in endothelial membrane integrity and permeability that may ultimately lead to pathophysiological outcomes (Lum and Roebuck 2001). One recent study revealed that the disturbance of these natural barriers led to increased vascular permeability and the entry of low-density lipoprotein (LDL) into subendothelial spaces, thereby promoting plaque formation, one of the initial events in the early stages of atherosclerosis (Gimbrone and García-Cardeña 2016).

Calpains (CAPNs) have been identified as a conserved family of intracellular calcium-sensitive cysteine proteases, with CAPN-1 (μ-CAPN) and CAPN-2 (m-CAPN) being the most ubiquitously expressed in various mammalian cell types and tissues (Huang and Wang 2001). CAPN activity is increased by calcium flux into the cytosol, whereas CAPN activity is down-regulated when these enzymes are bound by calpastatin (CAST), the endogenous inhibitor (Ono et al. 2016). CAPNs regulate multiple biological, processes including cell proliferation, adhesion, motility, and apoptosis through the functional cleavage of target proteins (Goll et al. 2003). Previous studies have revealed that CAPN activation plays an important role in atherogenesis by regulating endothelium functions, including apoptosis of endothelial cells, expression of adhesion molecules for immune cells, and barrier dysfunction (Miyazaki et al. 2013). For example,

Address correspondence to Zhi Huang, Department of Biotechnology, Jinan University, Guangzhou, Guangdong Province, China. Email: Thsh@jnu.edu.cn; Telephone: (86) 20-85220219

Supplemental Material is available online (https://doi.org/10.1289/EHP4538).

The authors declare they have no actual or potential competing financial interests.

Received 8 October 2018; Revised 31 May 2019; Accepted 7 June 2019; Published 5 July 2019.

Note to readers with disabilities: *EHP* strives to ensure that all journal content is accessible to all readers. However, some figures and Supplemental Material published in *EHP* articles may not conform to 508 standards due to the complexity of the information being presented. If you need assistance accessing journal content, please contact ehponline@niehs.nih.gov. Our staff will work with you to assess and meet your accessibility needs within 3 working days.

vascular endothelial cadherin (VE-cadherin), which serves as a major structural protein of adherence junctions and a structural mediator of endothelial integrity (Gavard 2009), was directly cleaved by CAPN-2, resulting in disorganized structures in aortic endothelial cells during atherosclerosis (Miyazaki et al. 2011).

Arsenic trioxide (ATO), a trivalent As compound, is released into the air and water through natural and industrial processes. It is the most commonly produced form of iAs that may generate arsenite in alkaline solutions (Huang et al. 2015). Although multiple As species have been used in As exposure studies involving animal and cell models, the use of low-dose ATO exposure has proven to be useful in studies of As-induced cardiovascular disorders (Mumford et al. 2007; Rahman et al. 2015). Considering the potential roles of As and CAPNs in endothelial cell functions, we hypothesized that endothelial dysfunction induced by As exposure may be mediated by CAPN activity. To address this issue, ATO was used to study the effects and mechanisms of As on endothelial dysfunction in mouse and human umbilical vein endothelial cell (HUVEC) models.

Materials and Methods

Mice and Exposure Protocol

The Animal Care and Ethics Committee of Jinan University approved the animal protocols (20150306003, 20180309001) in this study. C57BL/6J mice were obtained from the Experimental Animal Center of Southern Medical University (Guangzhou, China), and B6.129P2-*ApoE*^{tm1Unc}/J (ApoE$^{-/-}$) mice were purchased from Jackson Laboratories. All mice were housed five mice per cage and fed a normal diet *ad libitum* in an environmentally controlled room (21 ± 1°C with a 12-h photoperiod) in the Institute of Laboratory Animal Science, Jinan University. Three independent experiments were conducted with different cohorts of mice at 6–8 weeks of age. For long-term As exposure, male C57BL/6J mice were randomly assigned to four groups ($n = 30$ per group). The control group was maintained on tap water, whereas the three As exposure groups were maintained on tap water treated with 10 ppb As supplied by ATO (As_2O_3; 13.2 μg/L), arsenate pentoxide hydrate (arsenate; $As_2H_2O_6$, 16.5 μg/L), or roxarsone ($C_6H_6AsNO_6$; 35.1 μg/L) for 4 weeks. For short-term As exposure, two groups ($n = 20$ per group) of male C57BL/6J mice were maintained on tap water with or without ATO (10 ppb As) for 1 week. In addition, two groups ($n = 10$ per group) of either male ApoE$^{-/-}$ or male C57BL/6J mice [wild type (WT)] were assigned and treated with or without ATO for 4 weeks as above.

During long-term As exposure, body weights were measured weekly and changes in body weight for each group were expressed as average percentage (%) relative to initial weight. Drinking water was freshly prepared and changed every 3 d. To monitor water consumption per mouse, singly housed mice (five mice per group, one mouse per cage) were compared with group-housed mice (five mice per group, one cage per group) in the same room. Drinking water levels were measured every 3 d over a period of 4 weeks. Water consumption was expressed as milliliters per mouse per day averaged for every week (see Figure S1F) or the total time course (see Figure S1G). Water consumption was also compared between ApoE$^{-/-}$ and WT mice with or without ATO treatment (see Figure S3G). To account for differences due to fluid spillage (on average, 1.2 mL/d), a graduated cylinder with a drinking nipple was hung on an empty cage.

ATO, arsenate, and roxarsone were purchased from Sigma and represented the species of trivalent arsenite, pentavalent arsenate, and organoarsenicals, respectively, which are the major species involved in human exposure.

Vascular Permeability Assay

After exposure, mice vascular permeability was assessed by two end point experiments. First, mice ($n = 3$ per group) were injected intravenously with 200 μL of 0.5% sterile Evans blue dye (Sigma) via the tail vein. After 30 min, the mice were euthanized by carbon dioxide inhalation. The aortas, feet, and colons were dissected, weighed, and photographed. Evans blue dye was extracted from tissues using 0.5 mL formamide at 55°C for 24 h and measured at 610 nm as described in previous studies (Han et al. 2002). Second, mice ($n = 3$ per group) were injected intravenously with 200 μL of fluorescein isothiocyanate–labeled bovine serum albumin (FITC-BSA) (50 μg/μL; Sigma) via the tail vein. After 60 min, the mice were euthanized and the aortas were sampled and fixed in 4% paraformaldehyde overnight. Following dehydration in a series of alcohol baths and clearing in xylene, aortas were embedded in Paraplast® (Leica) and then cut into 5-μm sections using an automated microtome (model RM2255; Leica) that were then adhered immediately onto glass slides (CitoTest). After deparaffinization and rehydration, nuclei were counterstained with 4′,6-diamidino-2-phenylindole (DAPI; a blue-fluorescent DNA stain) (0.1 mg/mL; Sigma). Images of aortic sections were captured by EVOS® FL Imaging System (ThermoFisher) using the excitation and emission spectra 360/447 nm for DAPI and 470/525 nm for FITC-BSA. Relative fluorescence intensity of FITC-BSA in sections ($n = 3$ per mice) were quantified by ImageJ (version 1.46r; National Institutes of Health) (Schneider et al. 2012).

Cell Cultures and Treatment

HUVECs and THP-1 cells (a human monocytic cell line) were obtained from American Type Culture Collection (ATCC). HUVECs were cultured in Dulbecco's Modified Eagle Medium/Nutrient Mixture F-12 (DMEM/F-12) medium (Gibco), whereas THP-1 cells were cultured in Roswell Park Memorial Institute 1640 (RPMI-1640) medium (Gibco) and activated by phorbol 12-myristate 13-acetate (100 ng/mL; Cayman) treatment for 24 h. All culture media were supplemented with 10% fetal bovine serum (FBS; Gibco), penicillin (100 U/mL; Gibco), and streptomycin (100 μg/mL; Gibco). The cells were cultured at 37°C in a humidified 5% CO_2 atmosphere in an incubator (ESCO). Based on the experimental design, HUVECs were seeded in triplicate in 96-well plates (0.2×10^4 or 1×10^4 per well), in 6-well plates (2×10^5 per well), or in 10-cm dishes (2×10^7 per dish) and incubated overnight or for longer periods to reach suitable confluency. Generally, cells were exposed to As in culture medium for 24 h at a final concentration of As of 0.13 μM (equal to 10 ppb) supplied by the ATO stock solution (1.3 mM As), which was prepared by dissolving 13.2 mg of ATO in 100 mL of 0.1 M sodium hydroxide (NaOH; Sigma). Other stock solutions with 1.3 mM As for arsenicals including arsenate and roxarsone were also prepared in 0.1 M NaOH and diluted to their final concentrations of As using the complete culture media. The culture media with the same dilution of 0.1 M NaOH also served as the solvent control.

Cell Viability and Cell Growth

Cell viability and cell growth was detected using the Cell Counting Kit-8 (CCK-8; Dojindo). Briefly, HUVECs were seeded in triplicate in 96-well plates (1×10^4 per well), incubated overnight, and treated with ATO, arsenate, or roxarsone (0–4.16 μM As) for 24 h. Then, 10 μL of the CCK-8 solution was added and the cells were incubated for 2 h at 37°C. The absorbance was measured at 460 nm using a microplate reader (Synergy™ H1M; BioTek). For the cell proliferation assay, cells in 96-well plates (0.2×10^4 per well) were treated with ATO with

a series of dosages (0–4.16 μM As) for 0, 1, 3, and 6 d, and cell growth was assessed using the CCK-8 kit as above.

Flow Cytometry

HUVECs were seeded in triplicate in 6-well plates (2×10^5 per well) and treated with ATO as described above for flow cytometry analysis. The cells were harvested by trypsin (EDTA-free; Gibco) and washed twice with cold phosphate-buffered saline (PBS). Cell apoptosis was analyzed using the Annexin V-FITC/PI Kit (4A Biotech Co. Ltd) according to the manufacturer's instructions. The cells were resuspended in 100 μL binding buffer with 5 μL recombinant human Annexin V (FITC-labeled) for 5 min at room temperature (RT). Propidium iodide (PI; 10 μL, 20 μg/mL) was diluted in 400 μL PBS and added to each sample prior to analysis. A total of 2×10^4 events were analyzed by flow cytometer (NovoCyte®; ACEA) using the FL1 channel (488/530 nm) and the FL2 channel (488/570 nm). To analyze cell cycle distribution, the cells were fixed in 70% ethanol at −20°C overnight. After washing three times with PBS, the cells were stained with PI (10 μg/mL; Sigma) for 30 min at 4°C in the dark. Then 2×10^4 events were detected by flow cytometer using the FL2 channel. Unstained cells were used as negative controls, and each treatment was analyzed in three biological replicates.

Total Arsenic Detection and Arsenic Speciation Analysis

Total As (tAs) and As species were analyzed as described in a previous study (Li et al. 2018). Briefly, entire aortas ($n=3$ per group) were sampled, and HUVECs were harvested by a cell scraper washing with cold PBS after incubating in a 10-cm dish ($\sim4\times10^7$ per dish, $n=3$ per group) with ATO treatment (0, 0.13, 1.3, or 13 μM As) for the indicated times. Samples of aortas and cells were digested in 1.5 mL concentrated nitric acid (HNO_3; 67%) at RT for 30 min and then heated at 100°C after the addition of 1 mL concentrated hydrogen peroxide (H_2O_2; 30%) for another 3 h. After evaporating, samples were diluted with deionized water to 1 mL and subjected to inductively coupled plasma mass spectrometry with collision/reaction cell technology (ICP-CCT-MS; XSERIES® 2 ICP-MS equipped with CCT; ThermoFisher) for tAs detection.

To analyze As species, aortas and harvested cells were homogenized using a homogenizer (model OSE-Y50; Tiangen) on ice with 10 passes and ultrasonicated (VCX 130, Sonics & Materials) three times for 30 s on ice. The filtrates of the samples were collected by centrifugation at 14,000 rpm at 4°C for 20 min in an Ultra-0.5 Centrifugal Filter Unit (3 kDa, Amicon), and then subjected to an Ultimate 3,000 series high-pressure liquid chromatography (HPLC) system (ThermoFisher) with a CAPCELL PAK C18 column (5 μm, 4.6×250 mm; Shiseido) coupled to ICP-CCT-MS for As speciation analysis. Concentrations of tAs and As species in aortas or cells were normalized to protein concentrations of lysates, which were measured using a bicinchoninic acid (BCA) assay kit (Pierce). tAs and As species in culture media were also detected.

CAPN Activity Detection

CAPN activity was measured by using a CAPN activity assay kit (BioVision) according to the manufacturer's instructions. In brief, entire aortas ($n=3$ per group) or HUVECs seeded in 6-well plates ($\sim4\times10^6$ per well, $n=3$ per group) were homogenized and lysed in 200 μL extraction buffer on ice. Supernatants of lysates were collected by centrifugation at 12,000 rpm at 4°C for 1 min, and protein concentrations were detected by BCA assay. A mixture of cell lysates (containing 50 μg protein per assay) was diluted to 85 μL using the extraction buffer, and then 10 μL of 10× reaction buffer and 5 μL of CAPN substrates were added to each assay and incubated for 1 h at 37°C in the dark. Active CAPN (1 μL) or CAPN inhibitor (1 μL) was added to the mixture for positive control or negative control, respectively. Fluorescence intensity was measured using a microplate reader (Synergy™ H1M, BioTek) with a 400-nm excitation filter and a 505-nm emission filter. CAPN activity was expressed as relative fluorescence unit per milligram protein of each sample.

Active CAPN in Situ *Staining*

After short-term As exposure, activated CAPNs in aortas were visualized *in situ* by intravenous injection of the CAPN tracer, *t*-BOC-Leu-Met (20 μM; Invitrogen), 150 μL per mouse via the tail vein ($n=3$ per group). After 30 min, the mice were euthanized. Aortas were dissected, washed three times with cold PBS, and gross images of aortas ($n=3$ per group) were captured by using the fluorescence-labeled organism bioimaging instrument (FOBI) system (NeoScience) using the blue channel. As above, aortas were embedded in Paraplast® after fixation, dehydration, and clearing and then cut into 5-μm sections, which were adhered to glass slides. After deparaffinization and rehydration, sections ($n=3$ per aortas) were imaged by the EVOS® FL Imaging System using the excitation and emission spectra 360/447 nm. Relative fluorescence intensity in aortas and aortic sections were quantified by ImageJ 1.46r.

Intracellular Calcium Measurement

HUVECs were seeded in triplicate in 96-well plates (1×10^4 per well), incubated overnight, and co-cultured with or without ATO (0.13 μM As) for another 24 h. After pretreatment with or without the calcium chelator, BAPTA-AM (20 μM; Invitrogen), for 2 h, the fluorescent calcium indicator, Fura-2 AM, (2 μM; Invitrogen) was loaded in the medium for 45 min at 37°C. Then the cells were washed three times with PBS, and the fluorescence intensity was measured every 30 s using the Synergy™ H1M microplate reader equipped with 340- and 380-nm excitation filters and a 510-nm emission filter. Intracellular concentrations of calcium ($[Ca^{2+}]i$) were calculated using the Grynkiewicz equation as described in a previous study (Hirst et al. 2006):

$$[Ca^{2+}]i\,(nM) = K_d \times [(R - R_{min})/(R_{max} - R)] \times Sfb$$

For this equation, $R=340/380$ ratio and the normal value used for K_d is 225 nM. In this study, R_{max} (the 340/380 ratio under Ca^{2+}-saturating conditions), R_{min} (the 340/380 ratio under Ca^{2+}-free conditions), and *Sf*b (the ratio of baseline fluorescence under Ca^{2+}-free and -bound conditions at 380 nm) were 5.24, 0.73, and 1.91, respectively.

Measurement of Vascular Endothelial Cell Barrier

Cultured vascular endothelial cell monolayers were established by growing HUVECs on glass bottom dishes (NEST Biotech Co. Ltd.) or Transwell® permeability supports (Corning) as described in a previous study (Cancel and Tarbell 2011). Briefly, to assess the integrity of monolayers, HUVECs (2×10^5 per dish) were seeded in triplicate in glass bottom dishes to form monolayers. After treating with ATO (0.13 μM As) in the presence/absence of the CAPN-1 inhibitor, ALLM (10 μM), or the CAPN-2 inhibitor, Z-LLY-FMK (4 μM), for 24 h, the monolayers were stained with the lipophilic membrane dye, DiI (5 μM; Invitrogen), and the nucleic acid stain, Hoechst 33258 (1 μg/mL; Invitrogen), for 30 min. After washing three times with PBS, images were captured with a confocal laser scanning microscope (model FV10i; Olympus) using the excitation and emission spectra 359/461 nm

for Hoechst 33258 and 551/569 nm for DiI. Areas of intracellular gaps in three random fields for each treatment were quantified using ImageJ.

To assess the permeability of the macromolecules, monolayers were established by seeding HUVECs (5×10^4 per well) onto Transwell® permeable supports (0.4 μm pore size, 24-mm insert diameter; Corning) and treated as above. DiI-labeled ox-LDL (DiI-ox-LDL; 30 μg/mL; Yiyuan Biotech Co. Ltd.) was added to the inner chamber and the cells were incubated for another 24 h. The fluorescence intensity of DiI-ox-LDL in the outer chamber was detected using a Synergy™ H1M microplate reader with a 549-nm excitation filter and a 565-nm emission filter. Transendothelial electrical resistance (TEER) was detected at the indicated times using a Millicell® ERS-2 volt-ohm meter (Millipore) according to the user guide. To monitor changes in tAs and As species, the monolayers were treated with or without ATO (0.13 μM As) for 24 h and the media within the inner and outer chambers were collected for fluorescence detection at the indicated times ($n = 3$ per group).

To assess the permeability to transmigrating macrophages, monolayers were established by seeding HUVECs (1×10^4 per well) onto Transwell® permeable supports (8 μm pore size, 4.26 mm insert diameter; Corning) and treated as above. The media in the inner chambers were replaced with fresh medium containing 1% FBS and activated THP-1 cells (1×10^4 per well). After incubating for another 6 h, the monolayers and nonadherent THP-1 cells were gently scraped. THP-1 cells that had migrated into the membranes were visualized by staining with the membrane-permeable live-cell labeling dye, calcein-AM (1 μM; Invitrogen), DiI (5 μM), and Hoechst 33258 (1 μg/mL) for 30 min. After washing three times with PBS, images were captured with the EVOS® FL Imaging System using the excitation and emission spectra 470/525 nm for Calcium-AM, 360/447 nm for Hoechst 33258, and 530/593 nm for DiI. The total numbers of stained cells were counted manually in three random images per membrane ($n = 3$ per group).

Quantitative Polymerase Chain Reaction Analysis

Total RNA was isolated from aortas (~20 mg) or HUVECs (~4×10^6 cells) using the MiniBEST Universal RNA Extraction Kit (TaKaRa) following the manufacturer's instructions. A total of 1 μg isolated RNA for each sample was reverse transcribed with PrimeScript RT Master Mix (TaKaRa). Quantitative polymerase chain reaction (qPCR) was performed by using 2× SYBR® Green qPCR Master Mix (Bimake) and the LightCycler® 96 instrument (Roche) under the following parameters: 95°C for 5 min, 40 cycles at 95°C for 10 s, and 60°C for 30 s. To verify amplification specificity, a thermal denaturing cycle was added to derive the dissociation curve of the PCR product after amplification. The mRNA levels of target genes were calculated by the $2^{-\Delta\Delta CT}$ method using *beta-actin* as a housekeeping gene. Three biological replicates were analyzed for each group. All qPCR primers listed in Table S1 were designed using primer-BLAST (Ye et al. 2012) and obtained from Sangon Biotech Co. Ltd.

Western Blotting

Aortas (~20 mg) or treated cells (~4×10^6 cells) were homogenized and/or lysed in 150 μL of radioimmunoprecipitation assay (RIPA) buffer (ThermoFisher) containing a protease inhibitor cocktail (Sigma), and ultrasonicated as above. Supernatants of lysates were collected by centrifugation at 14,000 rpm at 4°C for 15 min, and protein concentrations were determined using the BCA assay. After adjusting to equal protein concentrations and boiling with Laemmli sample buffer (Bio-Rad), the protein samples were separated by sodium dodecyl sulfate–polyacrylamide gel electrophoresis (SDS-PAGE) and transferred to a polyvinylidene difluoride (PVDF) membrane (0.22 μm; Millipore). The membranes were blocked with 5% nonfat milk (BD) for 1 h and then incubated with the indicated primary antibodies overnight at 4°C. After washing three times with tris-buffered saline with 0.1% Tween® 20 (TBST) (Sigma) at 5-min intervals, the membranes were incubated with horseradish peroxidase–linked anti-rabbit antibody (diluted in 5% BSA/TBST with 1:3,000 dilution) (Cat. No. 7074S, Lot No. 27; Cell Signaling) for 1 h at RT. After washing three times with TBST at 10-min intervals, protein bands were visualized by a chemiluminescent imaging system (model 5200; Tanon) using electrochemiluminescence (ECL) assay kits (Pierce). Each group was analyzed in triplicate (biological replicates), and relative protein levels were quantified relative to β-actin by using the software ImageJ 1.46r.

The following primary antibodies, including anti-CAST (sc-20779, Lot No. J2513, 1:500; Santa Cruz), anti-CAPN-1 (ab39170, Lot No. GR299070-9, 1:1,000; Abcam), anti-CAPN-2 (ab39165, Lot No. GR299070-9, 1:1000; Abcam), anti-CAPNS1 (ab28237, Lot No. GR640370-7, 1:1,000; Abcam), anti-β-actin (4970S, Lot No. 15, 1:1,000; Cell Signaling), and anti-Na^+/K^+-ATPase (3010S, Lot No. 6, 1:1,000; Cell Signaling) were diluted in 5% BSA/TBST.

Membrane and Cytosol Protein Extraction

To determine CAPNs and CAST levels in cytosolic and membrane fraction, HUVECs (2×10^7 per dish) were seeded in triplicate in 10-cm dishes. After reaching full confluency, the cells were treated with ATO (0.13 μM As) for the indicated times. Cytosolic and membrane proteins were extracted using a membrane and cytosol protein extraction kit (Beyotime) according to the manufacturer's instructions. Protein levels were detected by SDS-PAGE and western blotting as described above. The relative levels of cytosolic proteins or membrane proteins were normalized to β-actin or Na^+/K^+-ATPase, respectively.

Immunofluorescence

Coverslips (14-mm diameter; NEST Biotech Co. Ltd) were coated with poly L-lysine (0.1 mg/mL; Sigma) for 1 h at 37°C, and washed three times with deionized water. HUVECs (2×10^5 per well) were seeded on coverslips in 24-well plates. To access the cellular distribution of CAPN-1, cells were treated with ATO (0.13 μM As) for the indicated times. The cells were fixed with 4% paraformaldehyde for 15 min, permeabilized with 0.2% Triton™ X-100 for 10 min and blocked with 10% goat serum for 1 h. The cells were then incubated with rabbit polyclonal antibody recognizing CAPN-1 (diluted in 2% goat serum/PBS with 1:100 dilution; ab28257; Abcam) overnight at 4°C. After washing with 0.1% Tween®-20/PBS, cells were incubated with Cy3-conjuated goat anti-rabbit IgG antibody (MO2284, diluted in 2% goat serum/PBS with 1:100 dilution; E031620; EarthOx) at RT for 1 h. After washing with 0.1% Tween®-20/PBS, DAPI was used for nuclei staining. After sealing with ProLong™ Gold antifade mountant (Cat. No. P36934; Invitrogen), images were captured by confocal laser scanning microscope using the excitation and emission spectra 359/461 nm for DAPI and 547/567 nm for Cy3.

To assess the proteolytic disorganization of VE-cadherin, cells were treated with ATO (0.13 μM As) in the presence/absence of ALLM (10 μM) or Z-LLY-FMK (4 μM) for 24 h until reaching full confluency. VE-cadherin in cells was detected using rabbit monoclonal antibody recognizing VE-cadherin (2500S;

diluted in 2% goat serum/PBS with 1:100 dilution) followed by Cy3-conjuated goat anti-rabbit IgG as above.

Transfection and siRNA

HUVECs (2×10^5 per well) were seeded in 6-well plates and transfected with CAPN-1 siRNA (sc-29885; Santa Cruz), CAPN-2 siRNA (sc-41459; Santa Cruz), CAST siRNA (sc-29885; Santa Cruz), or control siRNA (sc-37007; Santa Cruz) using TransIT-siQUEST Transfection Reagent (Mirus) following the manufacturer's instructions. After 24 h, gene silencing was confirmed by western blotting. The cells were then treated with or without ATO (0.13 μM As) for 24 h, and CAPN activity was detected. Each treatment was analyzed in triplicate (biological replicates).

Co-Immunoprecipitation

Co-immunoprecipitation of CAST and CAPNs was assessed using Dynabeads® Protein A (Invitrogen) according to the manufacturer's instructions. Dynabeads® Protein A were bound to the anti-CAST antibody in 0.1% Tween®-20/PBS for 10 min at RT. HUVECs (2×10^5 per well) were seeded in triplicate in 6-well plates and treated with ATO (0.13 μM As) for the indicated times. The cells were then lysed in 100 μL lysis buffer (Cell Signaling) containing phenylmethylsulfonyl fluoride (PMSF) (1 mM; Sigma). Supernatants of lysates were collected by centrifugation at 12,000 rpm at 4°C for 15 min and incubated with Dynabeads®-antibody complex overnight at 4°C. After washing three times with PBS, the Dynabeads® were eluted with glycine (50mM, pH 2.8; Sigma). Protein samples were neutralized with tris (1M, pH 8.5; Sigma), and boiled after adding Laemmli sample buffer. Targets, including CAST, CAPN-1, and CAPN-2, were detected using SDS-PAGE and western blotting, as described above.

Statistical Analysis

Experiments were performed a minimum of three independent trials. Results were analyzed using Prism software (version 6.01; GraphPad Software) and presented as mean ± standard deviation (SD). Unpaired Student's *t* tests were used to compare the means of two groups. One-way analysis of variance (ANOVA) was used for comparison of three or more groups and differences among the groups. When ANOVA was significant, post hoc testing of differences between groups was performed using the Tukey's honestly significant difference (HSD) test. For every figure, statistical tests are justified as appropriate. A $p < 0.05$ was considered statistically significant.

Results

Effects of Chronic Exposure to Arsenic on Vascular Permeability in Mice

Arsenite, arsenate, and roxarsone are major As species involved in human As exposure. To determine the effects of chronic exposure to these As species on vascular permeability *in vivo*, the mice were exposed to ATO, arsenate, or roxarsone through drinking water at 10 ppb As, which is the WHO limited guideline value (Seltenrich 2018) and the current Chinese standard for As in drinking water (Rodríguez-Lado et al. 2013). After a 4-week exposure, no differences in body weights (see Figure S1A) or water consumption (see Figure S1F–G) were found between the groups. In comparison with the control group, a light blue color appeared on the skin of ATO-treated mice around hairless tissues, including the nose, abdomen, and feet (Figure 1A, arrows), after intravenous injection with Evans blue dye. Aortas of ATO-treated mice exhibited Evans blue content (Figure 1B) with higher optical density values of the extracted dye (Figure 1C), which was consistent with the higher content in their colons (see Figure S1B–C) and feet (see Figure S1D–E). Similar assays were performed for vascular permeability by intravenous injection with FITC-BSA, where aortic sections from ATO-treated mice showed higher fluorescence intensity of FITC-BSA (5.11-fold; Figure 1D–E). In contrast, arsenate- or roxarsone-treated mice showed no obvious differences in vascular permeability using either Evans blue dye or FITC-BSA when compared with the control group. Concentrations of tAs and As species in aortas were also evaluated after a 4-week exposure to As. Although tAs accumulated in all As-exposure groups, only the accumulation of tAs in the aortas of ATO-treated mice was statistically significant (5.27 ng/g; see Figure S2A), in which iAs(III) was the major As metabolite (5.02 ng/g; see Figure S2B–C). Moreover, the effects of ATO on vascular permeability were further confirmed in $ApoE^{-/-}$ mice. Although a higher vascular permeability to Evans blue dye (3.09-fold; see Figure S3A–C) and FITC-BSA (1.96-fold; see Figure S3D–E) was observed in $ApoE^{-/-}$ mice exposed to ATO as well, no differences were found in comparison with WT mice exposed to ATO (see Figure S3).

Effects of ATO Treatment in HUVECs

Due to the greater vascular permeability that was found in ATO-treated mice, the effects of ATO treatment (0–4.16 μM) *in vitro* were further studied using HUVECs. Data showed that no significant differences in cell viability (Figure 2A), cell growth (see Figure S4A), cell apoptosis (see Figure S4B and Table S2), or cell cycle distribution (see Figure S4C and Table S3) were detected in HUVECs treated with ATO at As concentration of 0.13 μM (10 ppb As). In contrast, ATO treatment (≥1.04 μM As) exerted strong inhibitory effects on cell viability and cell growth along with the induction of cell apoptosis and cell cycle disruption. Moreover, the effects of ATO treatment on As metabolism in HUVECs were also evaluated. As shown in Figure 2B, tAs accumulated in increasing amounts and peaked at 12.15 ng/mg protein. The major As metabolite in HUVECs with a 24-h ATO treatment (0.13 μM As) was iAs(III) (11.50 ng/mg protein; Figure 2C–D), whereas iAs(V) was the main metabolite in the medium (6.11 ng/mL; Figure 2E–F).

Effects of ATO on CAPN Activation in Aortas and HUEVCs

It has been reported that As exposure activates CAPN proteolytic enzymes (Vahidnia et al. 2008). To investigate the potential role of CAPN in vascular endothelial dysfunction induced by ATO, the activity and expression levels of CAPNs in aortas were measured. Higher CAPN activity (149.2%; Figure 3A) and higher protein levels of CAPN-1 (1.60-fold; Figure 3B–C) were detected in the aortas of ATO-treated mice. No significant differences in mRNA levels of CAPN-1 (Figure 3D) or in mRNA and protein levels of CAST, CAPN-2, or CAPN-4 were found in comparison with the control group (Figure 3A–D). Consistent with the observations obtained after a 4-week exposure to ATO, higher levels of CAPN activity were also detected in the aortas of mice after a 1-d exposure to ATO, and the activity was sustained at a higher level through 7 d (Figure 3E). Therefore, *t*-BOC-Leu-Met was further employed to visualize activated CAPNs in aortas *in situ*, and higher fluorescence intensity of *t*-BOC-Leu-Met was observed in the aortas of ATO-treated mice, particularly in the aortic arches (Figure 3F–G, arrows) and endothelium (Figure 3H–I, arrows).

Similar results were observed in HUEVCs, where CAPN activity was higher in the cells treated with ATO (≥0.13 μM As;

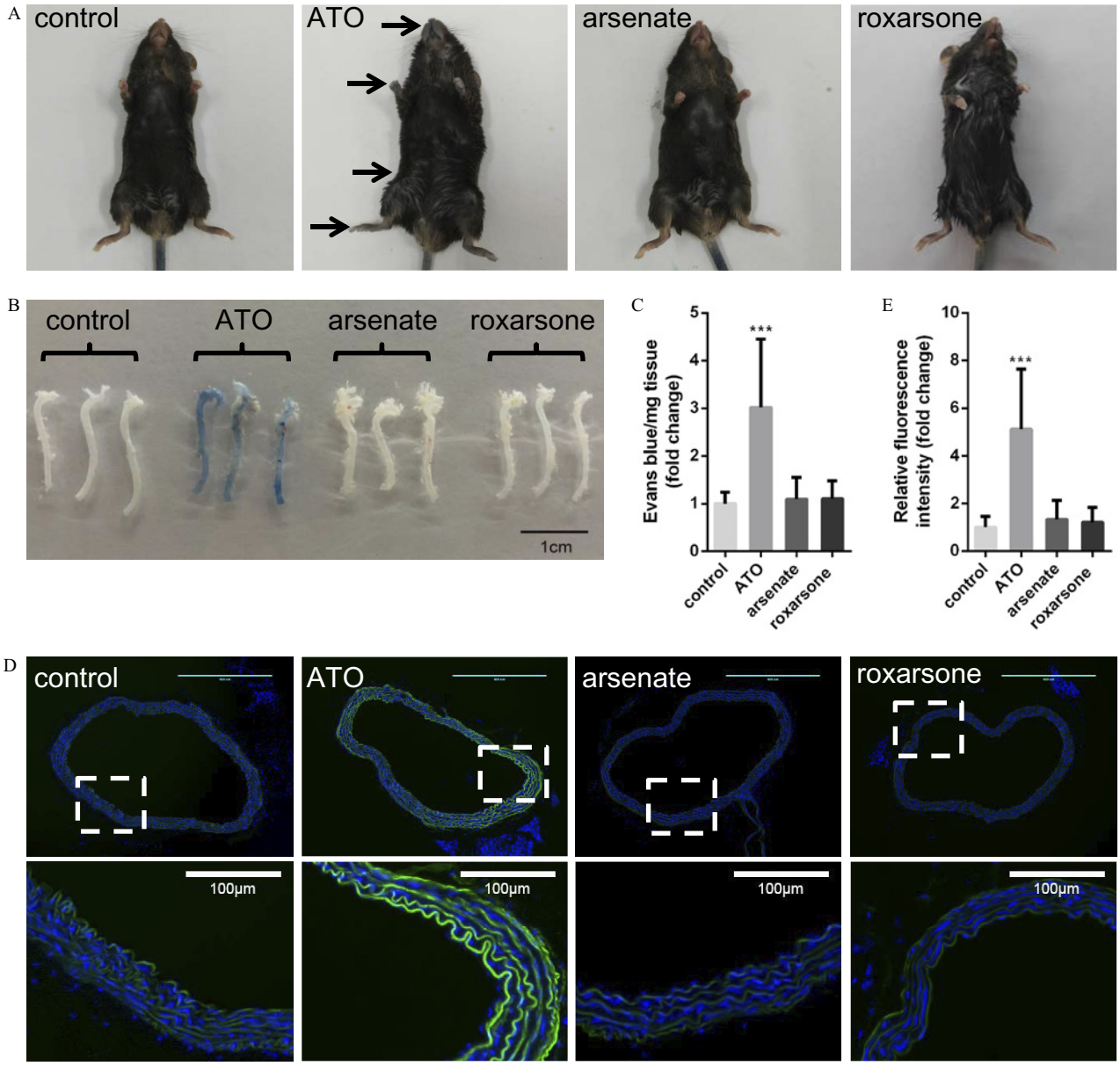

Figure 1. Vascular permeability in mice treated with 10 ppb of arsenic (As). Mice were randomly assigned to four groups ($n = 30$ per group) and exposed to 10 ppb As in drinking water supplied by arsenic trioxide (ATO), arsenic pentoxide (arsenate), or roxarsone or maintained on tap water for 4 weeks. Vascular permeability in mice was evaluated by intravenous injection with (A–C) Evans blue or (D–E) fluorescein isothiocyanate–labeled bovine serum albumin (FITC-BSA). Representative images of (A) mice or (B) aortas are shown. The arrows indicate blue coloration. Scale bar: 1 cm. (C) Evans blue dye in aortas was extracted and measured ($n = 3$ per group). (D) Representative images of FITC-BSA in aortic sections are shown (scale bar: 400 μm for top images and 100 μm for bottom images). (E) Relative fluorescence intensity of FITC-BSA in aortic sections was quantified by ImageJ (three sections per mouse; $n = 3$ mice per group). The data are presented as the mean ± standard deviation (SD). ***$p < 0.001$ compared with control using one-way ANOVA and Tukey post-test.

see Figure S5A). The peak response of CAPN activity in cells treated with ATO (0.13 μM As) occurred at 0.5 h (144.9%), followed by a decline that remained at a level above baseline (124.4%; Figure 4A). To determine how ATO activated CAPN, Fura-2 AM was used to evaluate effects of ATO on $[Ca^{2+}]i$. $[Ca^{2+}]i$ in HUEVCs treated with ATO increased rapidly from 39.2 nM to 105.5 nM but returned to the baseline level (Figure 4B). Cells pretreated with BAPTA exhibited a smaller increase in concentration of $[Ca^{2+}]i$ for a shorter length of time (Figure 4B) with no rapid activation of CAPN (Figure 4C) compared with the ATO-treated groups that were pretreated with dimethylsulfoxide (DMSO) or PBS. Next, to investigate the effects of ATO on mRNA and protein levels of CAPNs and CAST in HUVECs, qPCR and western blotting were employed, respectively. Compared with the control group, ATO-treated cells exhibited higher mRNA (149.7%; Figure 4D) and protein levels (2.46-fold; Figure 4E–F) of CAPN-1, accompanied by no significant differences in the mRNA and protein levels of CAPN-2, CAPN-4, and CAST (Figure 4D–F). In addition, specific siRNA targeting CAPN-1, CAPN-2, and CAST were then used to confirm their involvement in CAPN activation during ATO treatment in HUVECs. Gene silencing was confirmed (see Figure S5C, E, G), but only pretreatment with CAPN-1 siRNA resulted in an inhibitory effect on rapid CAPN activation after ATO treatment in comparison with the control siRNA-pretreated group (see Figure S5). To further detect whether interaction of CAST with CAPNs

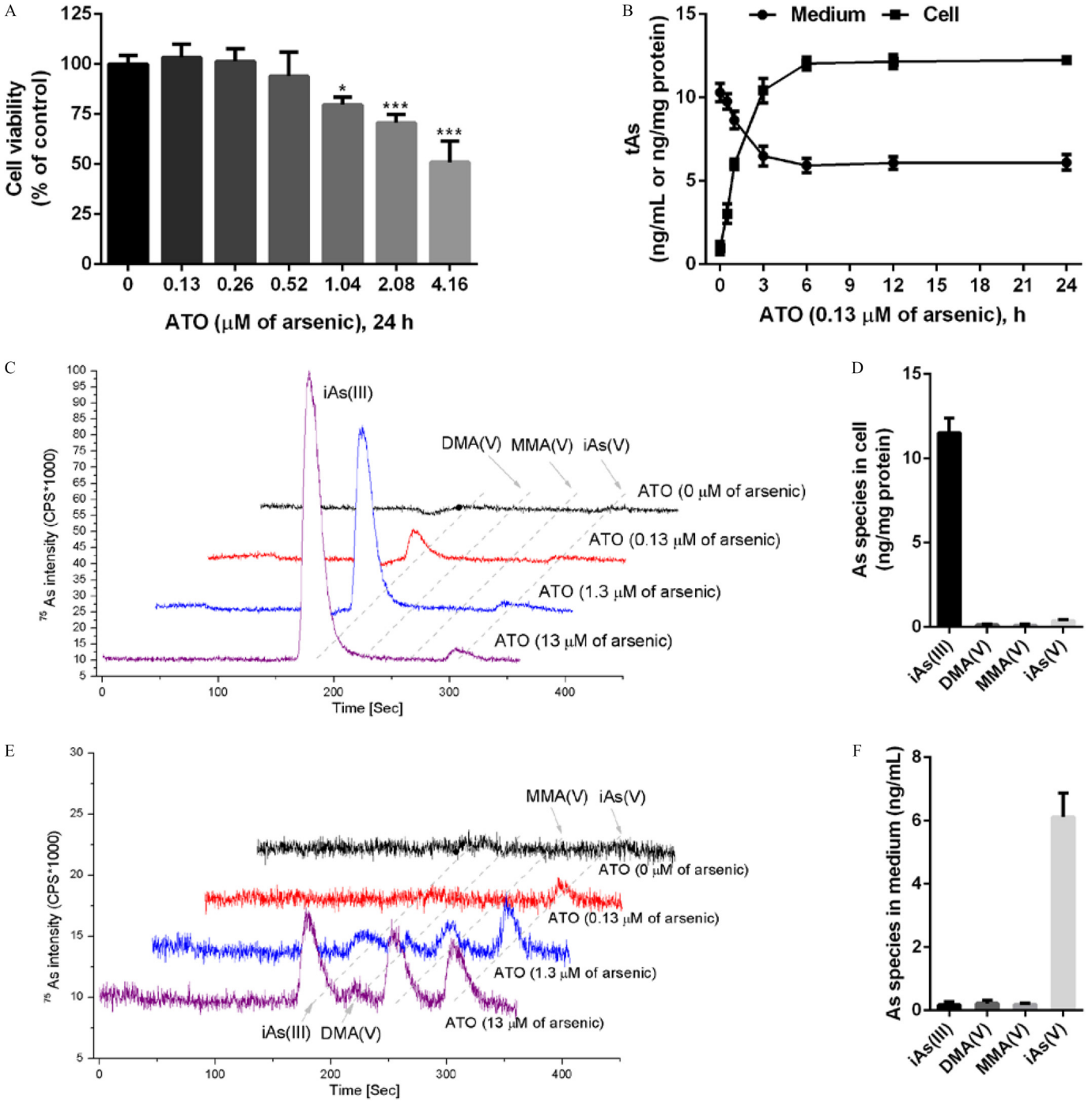

Figure 2. Dose effects of arsenic trioxide (ATO) on endothelial cells. (A) Human umbilical vein endothelial cells (HUVECs) were treated with ATO [0–4.16 μM of arsenic (As)] for 24 h, and cell viability was detected by using the Cell Counting Kit-8 (CCK-8) kit ($n = 3$ per group). (B) HUVECs were treated with ATO (0.13 μM As) for the indicated times and concentrations of total arsenic (tAs) was detected ($n = 3$ per group). The representative chromatograms of As species, including sodium arsenite [iAs(III)], sodium arsenate [iAs(V)], monomethylarsenic disodium [MMA(V)], and dimethylarsenic acid [DMA(V)], in (C) HUVECs or (E) medium after exposure to indicated doses of ATO for 24 h are shown. The concentrations of As species in (D) HUVECs or (F) medium after a 24-h ATO treatment (0.13 μM As) are shown ($n = 3$ per group). The data are presented as the mean ± standard deviation (SD). Note: ANOVA, analysis of variance. *$p < 0.05$ or ***$p < 0.001$ compared with the 0 μM ATO-treated group control using one-way ANOVA and Tukey post-test.

occurred in cells during ATO treatment, co-immunoprecipitation were employed. As shown in Figure S6, CAST showed a stronger interaction with CAPN-1 but not CAPN-2 for both short (0.5 h) and long (24 h) periods of times. In addition, the effects of arsenate or roxarsone were also evaluated in HUVECs, but neither showed effects on cell viability (see Figure S7A), activity (see Figure S7C), mRNA levels (see Figure S7B), or protein levels (see Figure S7D–G) of CAPNs at the same concentrations of As (0.13 μM).

Effects of ATO on Membrane Translocation of CAPN-1 in HUVECs

Because the membrane translocation of CAPNs is associated with their activation, subcellular fractionation assays were employed to analyze membrane and cytoplasmic levels of CAPNs. CAPN-1 exhibited higher levels in the membrane fraction of ATO-treated cells (1.65-fold), with no significant

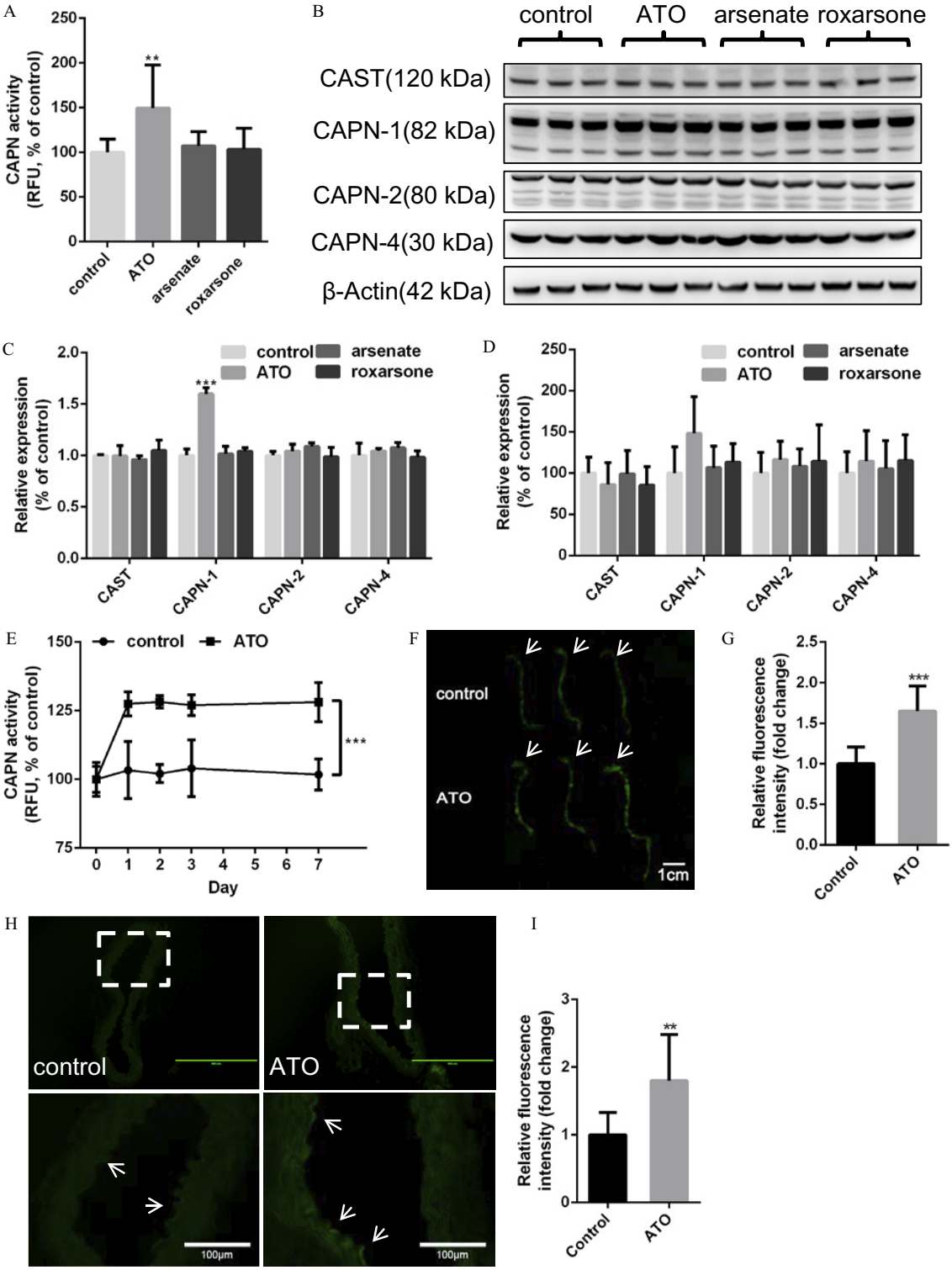

Figure 3. Calpain (CAPN) activity in the aortas of mice exposed to arsenic trioxide (ATO). (A–D) Mice were randomly assigned to four groups ($n = 30$ per group) and exposed to 10 ppb of arsenic (As) in drinking water supplied by ATO, arsenic pentoxide (arsenate), or roxarsone or maintained on tap water for 4 weeks. (A) CAPN activity in aortas was detected ($n = 3$ per group). (B) Protein levels of targets in aortas were analyzed by western blotting, and (C) relative protein levels normalized to β-actin are shown ($n = 3$ per group). (D) Relative mRNA levels of targets in aortas were quantified by qPCR ($n = 3$ per group). (E–I) Mice were randomly divided into two groups ($n = 20$ per group) and maintained on tap water with or without ATO supplementation (10 ppb As) for 1 week. (E) Mice were euthanized at indicated times and CAPN activity in aortas was detected ($n = 3$ per group). (F–I) Mice were injected intravenously with *t*-BOC-Leu-Met (20 μM). Representative images of active CAPNs (pseudocolored in green) in (F) aortas (scale bars: 1 cm) or (H) aortic sections (scale bars: 400 μm for top images and 100 μm for bottom images) are shown. Relative fluorescence intensity in (G) aortas ($n = 3$ per group) and (I) aortic sections (three sections per animal; $n = 3$ animals per group) were quantified by ImageJ. The data are presented as the mean ± standard deviation (SD). Note: ANOVA, analysis of variance; CAST, calpastatin; RFU, relative fluorescence unit; qPCR, quantitative polymerase chain reaction. $^{**}p < 0.01$ or $^{***}p < 0.001$ compared with control using one-way ANOVA and Tukey post-test.

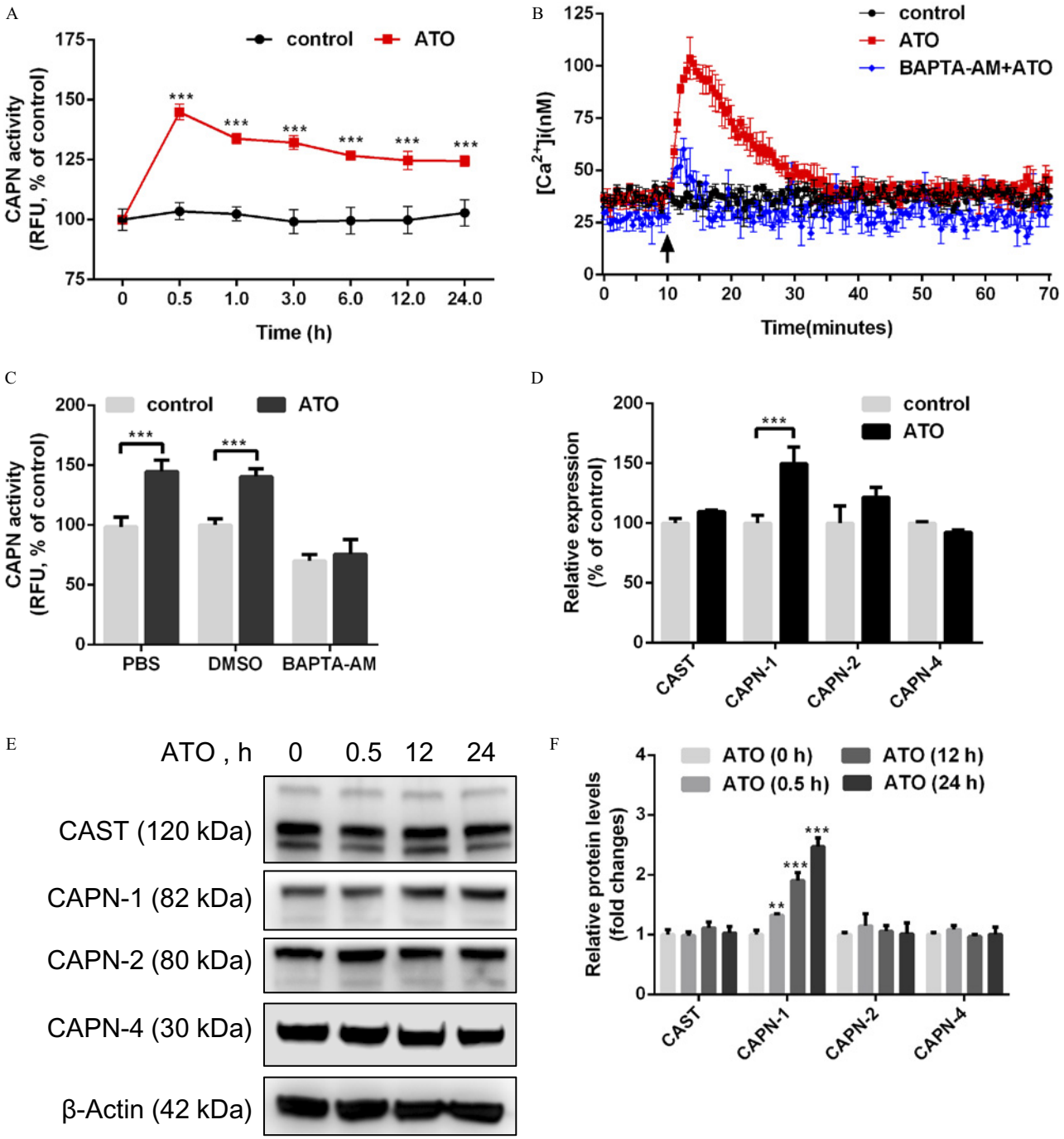

Figure 4. Calpain (CAPN) activity in human umbilical vein endothelial cells (HUVECs) treated with arsenic trioxide (ATO). (A) HUVECs were treated with ATO [0.13 μM of arsenic (As)] for 24 h, and CAPN activity was detected ($n = 3$ per group). HUVECs were treated with ATO (0.13 μM As) for (B) 1 h or (C) 0.5 h in the pretreatment with/without BAPTA-AM (20 μM, 2 h). (B) Intracellular calcium concentration ($[Ca^{2+}]i$) was measured by using Fura-2 AM and $[Ca^{2+}]i$ was calculated ($n = 3$ per group; arrow indicates ATO addition). (C) CAPN activity was detected ($n = 3$ per group). PBS and DMSO were served as solvent controls. (D) Gene expression of CAPNs or calpastatin (CAST) in HUVECs treated with ATO (0.13 μM As, 12 h) was assessed by qPCR ($n = 3$ per group). (E) Protein levels in HUVECs treated with ATO (0.13 μM As) for the indicated times were assessed by western blotting and (F) relative protein levels normalized to β-actin are shown ($n = 3$ per group). The data are presented as the mean ± standard deviation (SD). Note: ANOVA, analysis of variance; DMSO, dimethylsulfoxide; PBS, phosphate-buffered saline; RFU, relative fluorescence unit; qPCR, quantitative polymerase chain reaction. $^{**}p < 0.01$ or $^{***}p < 0.001$ compared with their own control using one-way ANOVA and Tukey post-test.

differences in the cytosolic fraction (Figure 5A–C). In addition, a greater increase in CAPN activity was detected in the membrane fractions (Figure 5D), although higher levels of CAPN activity was detected in both the cytosolic and membrane fractions of cells treated with ATO. Parallel experiments were performed to evaluate the effects of ATO on cellular distribution of CAPN-1 by using immunofluorescence. As shown in Figure 5E, foci of CAPN-1 were intensely localized to the cell surface of ATO-treated cells (arrows) compared with the untreated cells.

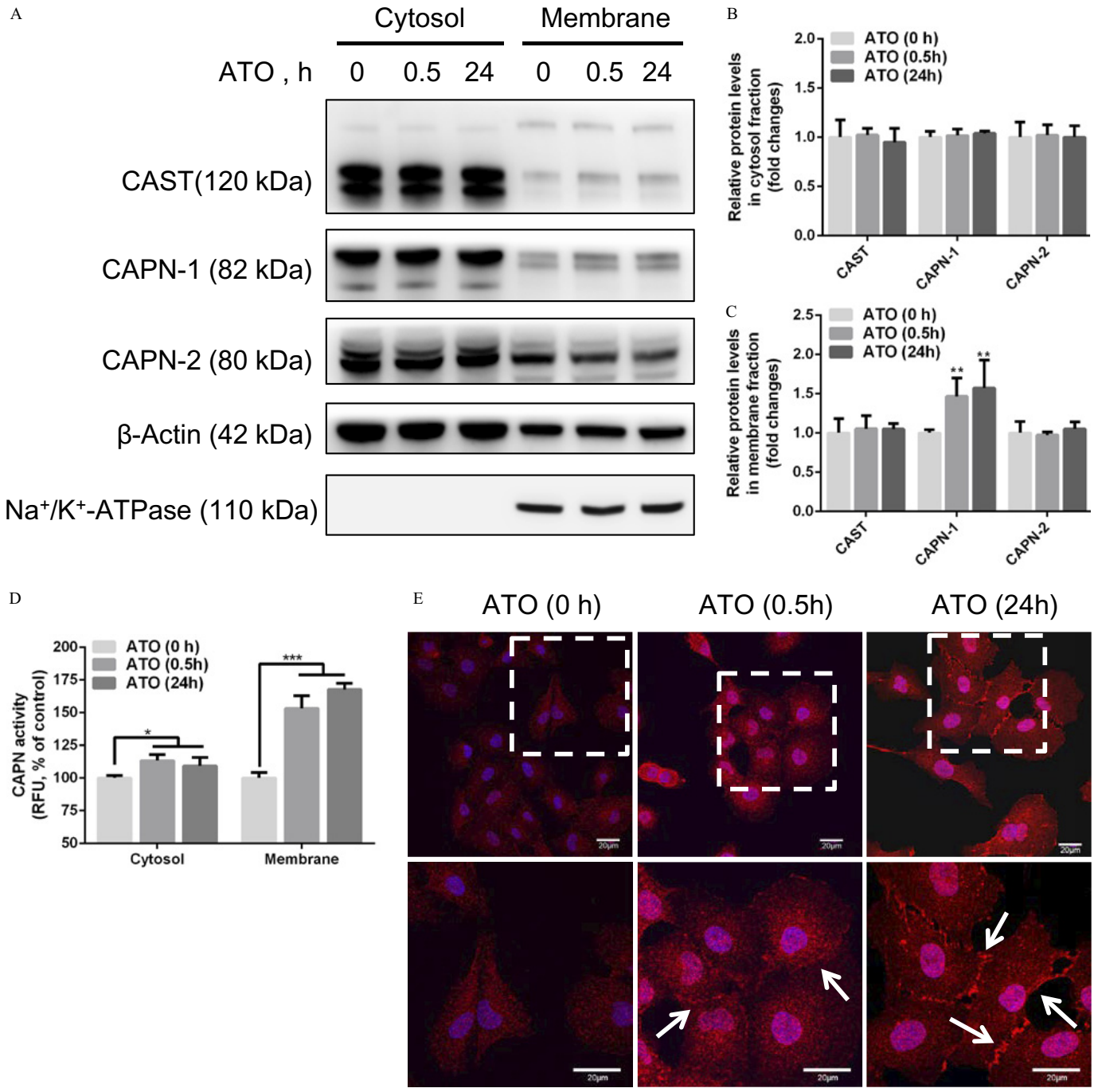

Figure 5. Protein levels and activity of calpains (CAPNs) in membrane fraction of human umbilical vein endothelial cells (HUVECs) treated with arsenic trioxide (ATO). HUVECs were treated with ATO [0.13 μM of arsenic (As)] for the indicated times. (A) Proteins levels of calpastatin (CAST) and CAPNs in cytosolic and membrane fractions were analyzed by western blotting. Relative protein levels in (B) cytosolic and (C) membrane fractions normalized to β-actin or Na^+/K^+-ATPase are shown ($n=3$ per group). (D) CAPN activity in different fractions was detected ($n=3$ per group). (E) CAPN-1 in cells treated with ATO (0.13 μM As) for the indicated times was detected a using rabbit polyclonal antibody followed by goat anti-rabbit antibody (Cy3-conjuated) and nuclei were counterstained with DAPI. Representative images are shown (scale bars: 20 μm) and arrows indicate foci of CAPN-1 in membrane. The data are presented as the mean ± standard deviation (SD). Note: ANOVA, analysis of variance; RFU, relative fluorescence unit. $*p<0.05$, $**p<0.01$, or $***p<0.001$ compared with control (0 h) using one-way ANOVA and Tukey post-test.

Effects of ALLM on Endothelial Function following ATO Treatment in Vitro

To further confirm the effects of ATO on endothelial dysfunction *in vitro*, HUVECs were used to establish cultured endothelial cell monolayers in a Transwell® system. Compared with the control group, ATO treatment resulted in intracellular gaps formation (arrows, 4.61%; Figure 6A–C), with gradual decreases in TEER of monolayers (Figure 6D). As expected, concentrations of tAs in the outer chamber and in the inner chamber tended to be equal (3.49 ng/mL; see Figure S8A) at 12 h and later after ATO treatment, and the major As species detected in both sides was iAs(V) after a 24-h treatment (see Figure S8B). To further determine the effects of ATO on the permeability of monolayers, the transendothelial transport of ox-LDL, and the transmigrating of activated THP-1 cells were measured. In comparison with the control

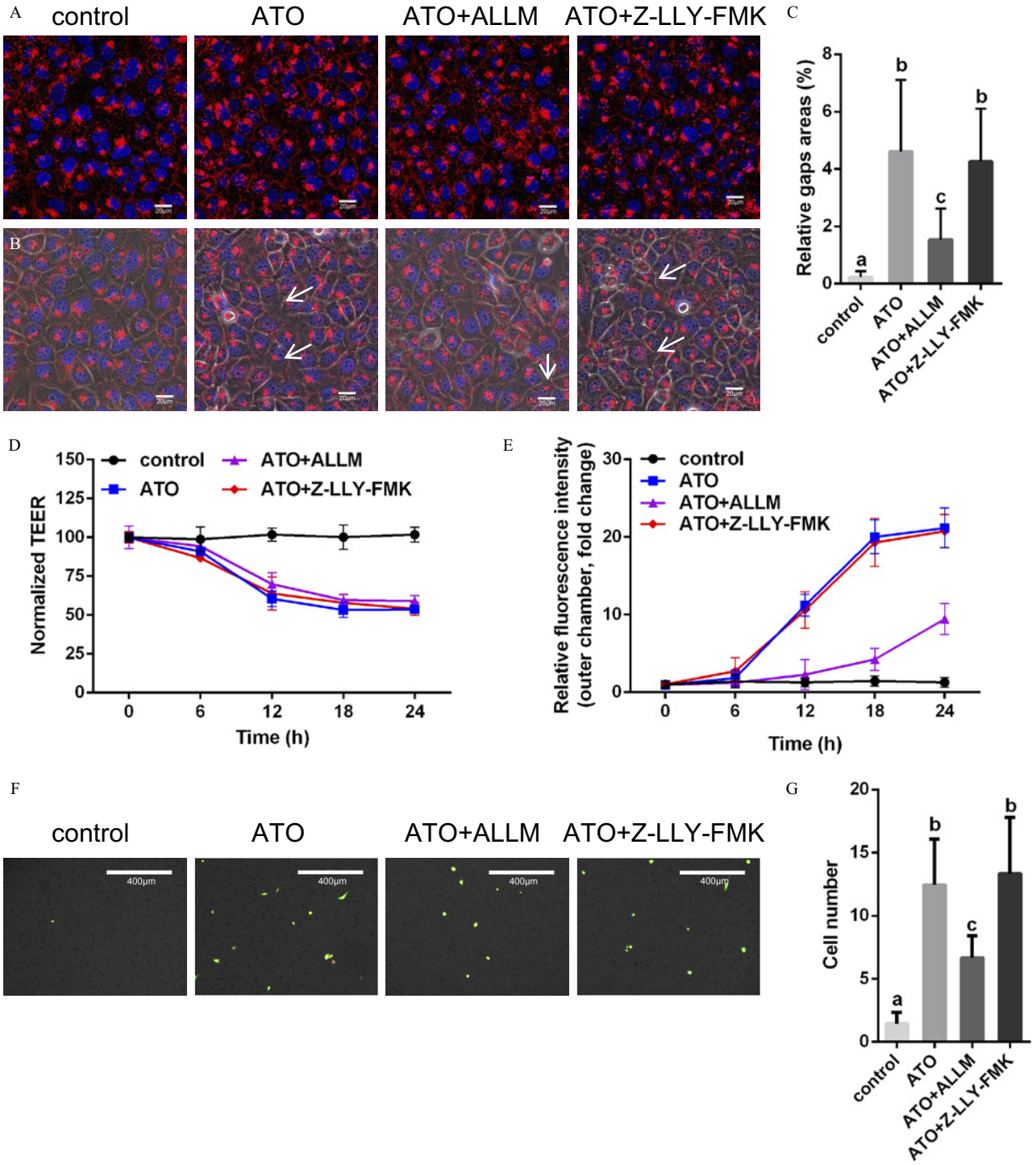

Figure 6. Effect of the CAPN-1 inhibitor, ALLM, on endothelial permeability in monolayers following arsenic trioxide (ATO)–treatment. Human umbilical vein endothelial cells (HUEVCs) were seed onto (A–C) glass bottom dishes or (D–G) Transwell® permeable supports to establish monolayers and then treated with ATO [0.13 μM of arsenic (As)] in the presence/absence of ALLM (10 μM) or the CAPN-2 inhibitor, Z-LLY-FMK, (4 μM) for 24 h. (A–B) Monolayers were stained with DiI and Hoechst. Representative (A) fluorescence images and (B) fluorescence images merged with the corresponding brightfield images are shown (scale bars: 20 μm; arrows indicate intracellular gaps). (C) Intracellular gaps were quantified as the percent area of monolayers uncovered by cells (three images per dish, $n = 3$ dishes per group). (D) Transendothelial electrical resistance (TEER) was detected at indicated times ($n = 3$ per group). Treated monolayers were co-cultured with (E) DiI-ox-LDL (30 μg/mL, 24 h) or (F–G) activated human monocytic cell line (THP-1) cells (1×10^4 per well, 6 h). (E) Relative fluorescence intensity of DiI-ox-LDL in the outer chamber was detected at indicated times ($n = 3$ per group). (F) Migrated THP-1 cells in membranes were stained with calcein-AM, DiI, and Hoechst, and representative images are shown (scale bars: 400 μm). (G) The total numbers of migrated cells were counted (three images per membrane, $n = 3$ membranes per group). The data are presented as the mean ± standard deviation (SD). Note: ANOVA, analysis of variance. Different letters indicate significant difference between groups ($p < 0.05$) as determined by one-way ANOVA and Tukey post-test.

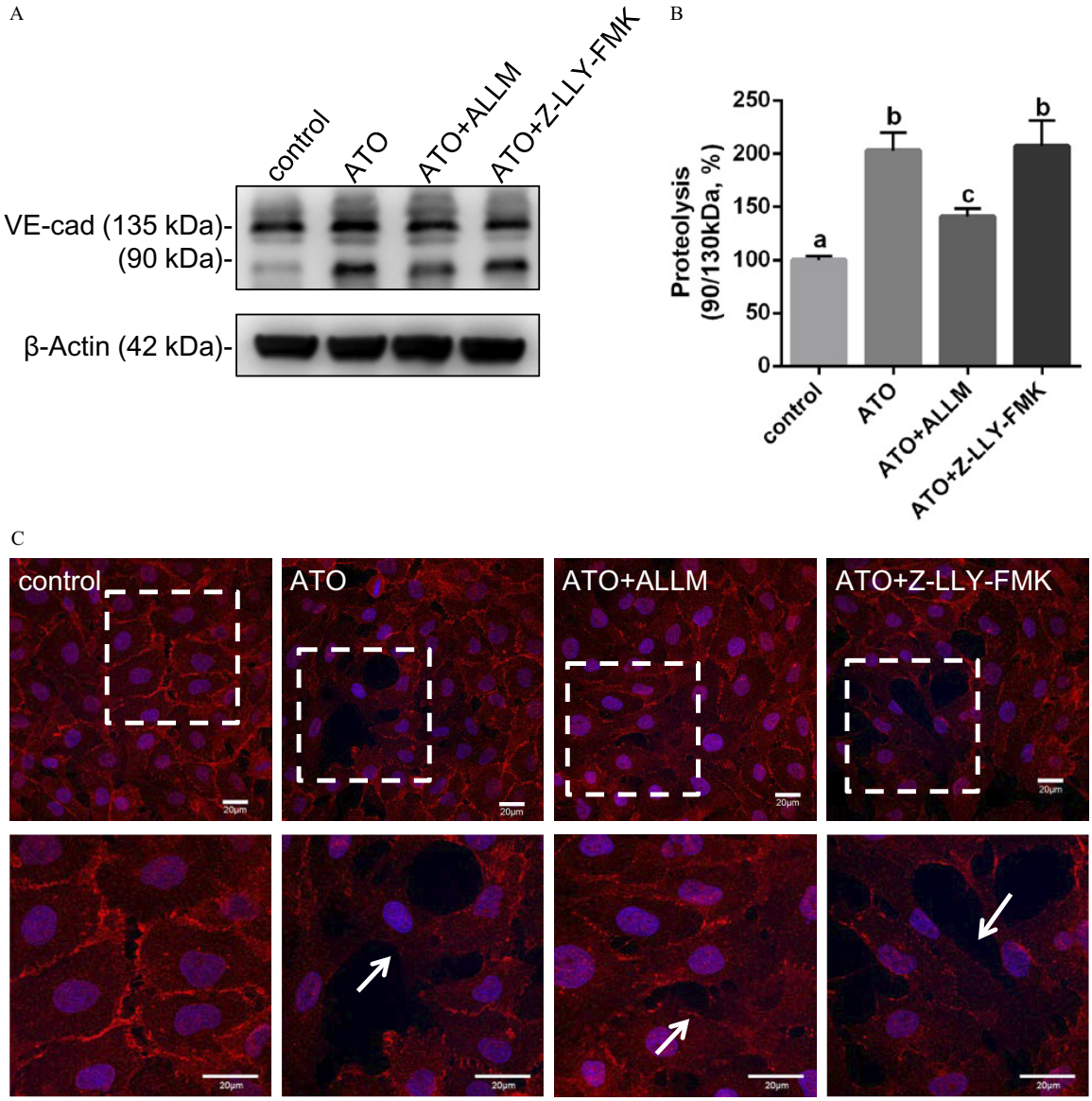

Figure 7. Effect of the CAPN-1 inhibitor, ALLM, on proteolysis of vascular endothelial cadherin (VE-cadherin) following arsenic trioxide (ATO)–treatment in human umbilical vein endothelial cells (HUVECs). HUVECs were treated with ATO [0.13 μM arsenic (As)] in the presence/absence of ALLM (10 μM) or the CAPN-2 inhibitor (Z-LLY-FMK) (4 μM) for 24 h. (A) Proteolysis of VE-cadherin was analyzed by western blot. (B) The graph represents the ratio of cleaved/uncleaved (90/135 kDa) bands of VE-cadherin ($n = 3$ per group). (C) VE-cadherin in cells was detected using rabbit monoclonal antibody followed by goat anti-rabbit antibody (Cy3-conjuated). Nuclei were counterstained with DAPI. Representative images are shown (scale bars: 20 μm), and arrow indicates proteolytic disorganization of VE-cadherin. The data are presented as the mean ± standard deviation (SD). Note: ANOVA, analysis of variance. Different letters indicate significant difference between groups ($p < 0.05$) as determined by one-way ANOVA and Tukey post-test.

group, the relative fluorescence intensity of DiI-ox-LDL in the outer chamber was markedly increased in the ATO-treated group (21.2-fold, 24 h; Figure 6E). Similarly, more THP-1 cells migrated transendothelially in membranes in the ATO-treated group as observed by fluorescent dye staining (Figure 6F–G).

To further evaluate the potential involvement of activated CAPN-1 in endothelial dysfunction during ATO treatment, assays were performed using inhibitors specific for CAPN-1 (ALLM) and CAPN-2 (Z-LLY-FMK). Compared with the ATO-treated group, smaller intracellular gaps (1.53%; Figure 6A–C), lower fluorescence intensity of DiI-ox-LDL in the outer chamber (9.45-fold; Figure 6E), and fewer THP-1 cells migrating transendothelially in membranes (Figure 6F–G) were observed in the combined ATO/ALLM treated group, with no difference in the TEER. In contrast, Z-LLY-FMK did not affect the gap formation or hyperpermeability of monolayers induced by ATO.

Effects of ALLM on CAPN Activation Induced by ATO

Next, mechanisms by which ALLM affected CAPN activation induced by ATO were investigated. Cells pretreated with ALLM had lower levels of CAPN activity in response to ATO compared with those treated with ATO alone (see Figure S9A), but they did not differ in CAPN protein levels (see Figure S9B–C) or in membrane translocation of CAPN-1 (see Figure S9D) in comparison with the ATO-treated group. Similar results were also detected in the combined ATO/Z-LLY-FMK–treated group (see Figure S9).

Effects of ALLM on Disorganization of VE-Cadherin following ATO Treatment in HUVECs

Disorganization of VE-cadherin catalyzed by CAPN during vascular hyperpermeability has been shown to play a fundamental role in atherosclerosis (Miyazaki et al. 2011). Therefore, effects of

ATO on this process were evaluated. Proteolysis of VE-cadherin was analyzed by western blotting. Both an intact band (135 kDa) and a fragmented band (90 kDa) of VE-cadherin were found in whole cell lysates. Compared with the control group, the ratio of 90/135 kDa bands was higher in the ATO-treated group (237.2%; Figure 7A–B). Combined ATO/ALLM treatment (121.8%), but not combined ATO/Z-LLY-FMK treatment (221.1%), showed a lower ratio of 90/135 kDa bands compared with the ATO-treated group. Immunofluorescence experiments were performed in parallel, and disorganization of VE-cadherin occurred in the cells treated with ATO, which could be partially blocked by treatment with ALLM but not Z-LLY-FMK (Figure 7C).

Discussion

Previous studies showed that As exposure could cause molecular and cellular events relevant to atherogenesis in cultured endothelial cells (Simeonova and Luster 2004) and also increase atherosclerotic plaque formation in $ApoE^{-/-}$ mice (Negro Silva et al. 2017). Epidemiological studies indicated that people exposed to low levels of As were prone to developing atherosclerosis (Ellinsworth 2015; Moon et al. 2013), but direct evidence on endothelial dysfunction has been lacking. In the present study, we found that exposure to ATO induced vascular endothelial dysfunction in mice and in cultured endothelial cell monolayers and was associated with the proteolytic disorganization of VE-cadherin and increased CAPN activation. Activation of CAPN during endothelial dysfunction induced by ATO was associated with increased $[Ca^{2+}]i$ and with increases in both protein levels and membrane translocation of CAPN-1.

ATO is generated and introduced into the atmosphere and water by natural and anthropogenic processes, posing a severe risk to global health (Pinto and Bennett 1963). In alkaline solutions or at low concentrations, ATO exists as arsenite, which is the prevalent metabolite of iAs in groundwater (Huang et al. 2015). Therefore, ATO was used as the representative form of arsenite in the present study, and it was found to induce vascular dysfunction in mouse aortas and cultured endothelial cell monolayers at the concentrations as low as 10 ppb of As, which is the WHO guideline value for safe values of As in drinking water (Seltenrich 2018). In addition, arsenate pentoxide (representative of arsenate) and roxarsone (an organic As additive widely used in the poultry industry, especially in Guangdong Province, China) were used for comparison in this study, but neither induced vascular endothelial dysfunction in mice (Figure 1A–D; see also Figure S1A–E).

The cardiovascular system may be much more sensitive to As exposure (Padovani et al. 2010), and cross-sectional studies showed that a less efficient As metabolism profile [higher percentage monomethylarsenic disodium (MMA%), lower percentage dimethylarsenic acid (DMA%)] was identified as a risk factor for cardiometabolic disease, including atherosclerosis, in humans (Chen et al. 2013; YR Huang et al. 2007; YL Huang et al. 2009; Spratlen et al. 2018). Compared with arsenate and roxarsone, more tAs accumulated (see Figure S2A) in the aortas of ATO-treated mice, consistent with the previous observation of the relatively higher cellular uptake and accumulation of arsenite in Caco-2 cells (human intestinal epithelial cells) (Liu et al. 2016). Similar results were observed in HUVECs treated with ATO (0.13 μM As), which was taken up quickly (Figure 2B) and accumulated in endothelial cells in the form of As(III) (Figure 2C–D) but was released into the media in the form of As(V) (Figure 2E–F). Notably, a less efficient As metabolism profile was found in cells treated with ATO (≥0.13 μM As). However, ATO at the levels used in this study (0.13 μM As) was previously defined as a low dose (Chen et al. 1997) and produced no significant cytotoxic effects on cell viability (Figure 2A), cell proliferation (see Figure S4A), or apoptosis (see Figure S4B) or on the cell cycle (see Figure S4C). This suggested that endothelial toxicity may not be the contributing factor to the vascular endothelial dysfunction mediated by ATO at such low levels.

CAPNs play important roles in inducing apoptosis for multiple cell types, in the cleavage of junction proteins, and in the expression of adhesion molecules during atherosclerosis (Miyazaki et al. 2013). ATO was shown to induce CAPN activation during apoptosis in neuroblastoma cells (Karlsson et al. 2007). Thus, we hypothesized that the pathological effects of ATO on endothelial cells may be exerted through CAPN activation. Our results showed that CAPN activity was higher in the aortas of ATO-treated mice (Figure 3A–I) as well as in endothelial cells treated with ATO and that the activity rapidly increased in cells over time with a peak response (Figure 4A–B), suggesting that the potential proteolytic effects were not transient in nature.

CAPN-1 and CAPN-2 are the two main isoforms of CAPNs that require binding to micromolar and millimolar levels of Ca^{2+} for activity, respectively (Huang et al. 2011). Previous studies showed that ATO could induce sustained increases in $[Ca^{2+}]i$ (Florea et al. 2007). In our study, we found that ATO also induced rapid increases in $[Ca^{2+}]i$ (Figure 4B) in HUVECs, accompanied by induced CAPN activity, which was confirmed by using BAPTA, the calcium chelator (Figure 4B–C). Moreover, ATO-treated cells exhibited higher mRNA (Figure 4D) and protein (Figure 4E–F) levels of CAPN-1, which was further shown to be the main contributor for CAPN activation during ATO treatment by RNA interference (see Figure S5B–H). This may be due to the higher sensitivity and lower requirement of CAPN-1 to $[Ca^{2+}]i$. Moreover, ALLM showed the capacity to inhibit CAPN activity in HUVECs (see Figure S9A), and it exerted mitigative effects on gap formation and hyperpermeability of cultured monolayers induced by ATO (Figure 6A–G), but it did not affect protein expression or membrane translocation of CAPN-1 (see Figure S9B–D). These collective data suggest that ATO induces endothelial dysfunction through CAPN-1 activation and support the notion that CAPN-2 plays less of a role.

Membrane association, autolysis, and phosphorylation all contribute to the activation of CAPNs (Goll et al. 2003; Storr et al. 2011). The importance of such an intricate system of regulation is due to the irreversible nature of CAPN proteolysis and the wide variety of cellular targets (Huang et al. 2013; Rose et al. 2015). Several membrane-associated proteins were identified as specific activators for CAPN-1 (Storr et al. 2011). Related to these issues, our results showed that compared with controls, ATO-treated cells showed higher levels of CAPN-1 and CAPN activity in the membrane fraction. As the endogenous inhibitor of CAPNs, CAST associates with active and inactive CAPN to control the overactivation of CAPNs (Melloni et al. 2006). Our preliminary results from co-IPs showed that interaction of CAST with CAPN-1 in cells exposed to ATO was higher (see Figure S6), which might explain the decline in CAPN activity over 24 h. Interaction of trivalent arsenicals and the sulfhydryl groups of proteins alters protein–protein interactions (Shen et al. 2013), but further studies are needed to prove that ATO induces impaired interaction of CAST with CAPN-1 by directly interacting with CAST or CAPN-1.

Our data show that VE-cadherin is a downstream target of CAPN-1 in endothelial cells during endothelial dysfunction induced by ATO (Figure 7A–C). Our results stand somewhat in contrast to earlier reports that CAPN-2 selectively carried out proteolysis of VE-cadherin, leading to barrier dysfunction of aortic endothelial cells during atherosclerosis (Gavard 2009;

Miyazaki et al. 2011). It may be that the location of the endothelial cells (e.g., in the aorta vs. small vessels) determines which CAPN mediates the permeability induced by ATO involving CAPN-mediated cleavage of junctional protein, including VE-cadherin.

In conclusion, these data from mouse models and an established endothelial monolayer model demonstrate that ATO-induced vascular endothelial dysfunction is mediated by increased CAPN-1 activity. This increased activity is associated with a rapid rise in $[Ca^{2+}]$i, increased CAPN-1 levels, and membrane localization of CAPN-1, which lead to increased proteolytic disorganization of VE-cadherin. The present data support the notion that therapeutics targeting CAPN-1 may be useful in attenuating atherogenesis induced by As exposure.

Acknowledgments

We thank B. Hu, M. He, and K. Nan (Key Laboratory of Analytical Chemistry for Biology and Medicine, Department of Chemistry, Wuhan University, PR China) for help with the total arsenic detection and arsenic speciation analysis. This work was supported by the National Natural Science Foundation of China (grants 81570397 and 81870323), the Project of Science and Technology of Guangdong (grants 2018A050506041 and A201501C07), the Major Project of Science and Technology of Guangzhou (grant 201604020142), and the Project of Virus Biology Laboratory of Guangzhou (grant 201705030003).

Reference

Bazzoni G, Dejana E. 2004. Endothelial cell-to-cell junctions: molecular organization and role in vascular homeostasis. Physiol Rev 84(3):869–901, PMID: 15269339, https://doi.org/10.1152/physrev.00035.2003.

Cancel LM, Tarbell JM. 2011. The role of mitosis in LDL transport through cultured endothelial cell monolayers. Am J Physiol Heart Circ Physiol 300(3):H769–H776, PMID: 21169397, https://doi.org/10.1152/ajpheart.00445.2010.

Chen GQ, Shi XG, Tang W, Xiong SM, Zhu J, Cai X, et al. 1997. Use of arsenic trioxide (As_2O_3) in the treatment of acute promyelocytic leukemia (APL): I. As_2O_3 exerts dose-dependent dual effects on APL cells. Blood 89(9):3345–3353, PMID: 9129041.

Chen Y, Wu F, Graziano JH, Parvez F, Liu M, Paul RR, et al. 2013. Arsenic exposure from drinking water, arsenic methylation capacity, and carotid intima-media thickness in Bangladesh. Am J Epidemiol 178(3):372–381, PMID: 23788675, https://doi.org/10.1093/aje/kwt001.

Ellinsworth DC. 2015. Arsenic, reactive oxygen, and endothelial dysfunction. J Pharmacol Exp Ther 353(3):458–464, PMID: 25788710, https://doi.org/10.1124/jpet.115.223289.

Florea A-M, Splettstoesser F, Büsselberg D. 2007. Arsenic trioxide (As_2O_3) induced calcium signals and cytotoxicity in two human cell lines: SY-5Y neuroblastoma and 293 embryonic kidney (HEK). Toxicol Appl Pharmacol 220(3):292–301, PMID: 17376498, https://doi.org/10.1016/j.taap.2007.01.022.

Gavard J. 2009. Breaking the VE-cadherin bonds. FEBS Lett 583(1):1–6, PMID: 19059243, https://doi.org/10.1016/j.febslet.2008.11.032.

Gimbrone MA Jr, García-Cardeña G. 2016. Endothelial cell dysfunction and the pathobiology of atherosclerosis. Circ Res 118(4):620–636, PMID: 26892962, https://doi.org/10.1161/CIRCRESAHA.115.306301.

Goll DE, Thompson VF, Li H, Wei W, Cong J. 2003. The calpain system. Physiol Rev 83(3):731–801, PMID: 12843408, https://doi.org/10.1152/physrev.00029.2002.

Han ED, MacFarlane RC, Mulligan AN, Scafidi J, Davis AE III. 2002. Increased vascular permeability in C1 inhibitor-deficient mice mediated by the bradykinin type 2 receptor. J Clin Invest 109(8):1057–1063, PMID: 11956243, https://doi.org/10.1172/JCI14211.

Hirst RA, Harrison C, Hirota K, Lambert DG. 2006. Measurement of [Ca2+]i in whole cell suspensions using fura-2. Methods Mol Biol 312:37–45, PMID: 16422189.

Huang CF, Yang CY, Chan DC, Wang CC, Huang KH, Wu CC, et al. 2015. Arsenic exposure and glucose intolerance/insulin resistance in estrogen-deficient female mice. Environ Health Perspect 123(11):1138–1144, PMID: 25859628, https://doi.org/10.1289/ehp.1408663.

Huang Y, Wang KK. 2001. The calpain family and human disease. Trends Mol Med 7(8):355–362, PMID: 11516996, https://doi.org/10.1016/S1471-4914(01)02049-4.

Huang YK, Tseng CH, Huang YL, Yang MH, Chen CJ, Hsueh YM. 2007. Arsenic methylation capability and hypertension risk in subjects living in arseniasis-hyperendemic areas in southwestern Taiwan. Toxicol Appl Pharmacol 218(2):135–142, PMID: 17173945, https://doi.org/10.1016/j.taap.2006.10.022.

Huang YL, Hsueh YM, Huang YK, Yip PK, Yang MH, Chen CJ. 2009. Urinary arsenic methylation capability and carotid atherosclerosis risk in subjects living in arsenicosis-hyperendemic areas in southwestern Taiwan. Sci Total Environ 407(8):2608–2614, PMID: 19187952, https://doi.org/10.1016/j.scitotenv.2008.12.061.

Huang Z, Hoffmann FW, Norton RL, Hashimoto AC, Hoffmann PR. 2011. Selenoprotein K is a novel target of m-calpain, and cleavage is regulated by Toll-like receptor-induced calpastatin in macrophages. J Biol Chem 286(40):34830–34838, PMID: 21849499, https://doi.org/10.1074/jbc.M111.265520.

Huang Z, Rose AH, Hoffmann FW, Hashimoto AS, Bertino P, Denk T, et al. 2013. Calpastatin prevents NF-κB-mediated hyperactivation of macrophages and attenuates colitis. J Immunol 191(7):3778–3788, PMID: 23986533, https://doi.org/10.4049/jimmunol.1300972.

Jomova K, Jenisova Z, Feszterova M, Baros S, Liska J, Hudecova D, et al. 2011. Arsenic: toxicity, oxidative stress and human disease. J Appl Toxicol 31(2):95–107, PMID: 21321970, https://doi.org/10.1002/jat.1649.

Karlsson J, Pietras A, Beckman S, Pettersson HM, Larsson C, Påhlman S. 2007. Arsenic trioxide-induced neuroblastoma cell death is accompanied by proteolytic activation of nuclear Bax. Oncogene 26(42):6150–6159, PMID: 17404572, https://doi.org/10.1038/sj.onc.1210439.

Korte NE, Fernando Q. 1991. A review of arsenic (III) in groundwater. Crit Rev Environ Control 21(1):1–39, https://doi.org/10.1080/10643389109388408.

Li Y, Chen B, He M, Hu B. 2018. Biomethylation metabolism study of arsenite in SCC-7 cells by reversed phase ion pair high performance liquid chromatography-inductively coupled plasma-mass spectrometry. Talanta 188:210–217, PMID: 30029366, https://doi.org/10.1016/j.talanta.2018.05.088.

Liu Q, Leslie EM, Le XC. 2016. Accumulation and transport of roxarsone, arsenobetaine, and inorganic arsenic using the human immortalized Caco-2 cell line. J Agric Food Chem 64(46):8902–8908, PMID: 27790904, https://doi.org/10.1021/acs.jafc.6b03341.

Lum H, Roebuck KA. 2001. Oxidant stress and endothelial cell dysfunction. Am J Physiol Cell Physiol 280(4):C719–C741, PMID: 11245588, https://doi.org/10.1152/ajpcell.2001.280.4.C719.

Melloni E, Averna M, Stifanese R, De Tullio R, Defranchi E, Salamino F, et al. 2006. Association of calpastatin with inactive calpain: a novel mechanism to control the activation of the protease? J Biol Chem 281(34):24945–24954, PMID: 16803906, https://doi.org/10.1074/jbc.M601449200.

Miller WH Jr, Schipper HM, Lee JS, Singer J, Waxman S. 2002. Mechanisms of action of arsenic trioxide. Cancer Res 62(14):3893–3903, PMID: 12124315.

Miyazaki T, Koya T, Kigawa Y, Oguchi T, Lei XF, Kim-Kaneyama JR, et al. 2013. Calpain and atherosclerosis. J Atheroscler Thromb 20(3):228–237, PMID: 23171729, https://doi.org/10.5551/jat.14787.

Miyazaki T, Taketomi Y, Takimoto M, Lei XF, Arita S, Kim-Kaneyama JR, et al. 2011. m-Calpain induction in vascular endothelial cells on human and mouse atheromas and its roles in VE-cadherin disorganization and atherosclerosis. Circulation 124(23):2522–2532, PMID: 22064597, https://doi.org/10.1161/CIRCULATIONAHA.111.021675.

Moon KA, Guallar E, Umans JG, Devereux RB, Best LG, Francesconi KA, et al. 2013. Association between exposure to low to moderate arsenic levels and incident cardiovascular disease. A prospective cohort study. Ann Intern Med 159(10):649–659, PMID: 24061511, https://doi.org/10.7326/0003-4819-159-10-201311190-00719.

Mumford JL, Wu K, Xia Y, Kwok R, Yang Z, Foster J, et al. 2007. Chronic arsenic exposure and cardiac repolarization abnormalities with QT interval prolongation in a population-based study. Environ Health Perspect 115(5):690–694, PMID: 17520054, https://doi.org/10.1289/ehp.9686.

Naujokas MF, Anderson B, Ahsan H, Aposhian HV, Graziano JH, Thompson C, et al. 2013. The Broad scope of health effects from chronic arsenic exposure: update on a worldwide public health problem. Environ Health Perspect 121(3):295–302, PMID: 23458756, https://doi.org/10.1289/ehp.1205875.

Negro Silva LF, Lemaire M, Lemarié CA, Plourde D, Bolt AM, Chiavatti C, et al. 2017. Effects of inorganic arsenic, methylated arsenicals, and arsenobetaine on atherosclerosis in the apoE$^{-/-}$ mouse model and the role of As3mt-mediated methylation. Environ Health Perspect 125(7):077001, PMID: 28728140, https://doi.org/10.1289/EHP806.

Ono Y, Saido TC, Sorimachi H. 2016. Calpain research for drug discovery: challenges and potential. Nat Rev Drug Discov 15(12):854–876, PMID: 27833121, https://doi.org/10.1038/nrd.2016.212.

Padovani AM, Molina MF, Mann KK. 2010. Inhibition of liver X receptor/retinoid X receptor-mediated transcription contributes to the proatherogenic effects of arsenic in macrophages in vitro. Arterioscler Thromb Vasc Biol 30(6):1228–1236, PMID: 20339114, https://doi.org/10.1161/ATVBAHA.110.205500.

Peters BA, Hall MN, Liu X, Parvez F, Sanchez TR, van Geen A, et al. 2015. Folic acid and creatine as therapeutic approaches to lower blood arsenic: a randomized controlled trial. Environ Health Perspect 123(12):1294–1301, PMID: 25978852, https://doi.org/10.1289/ehp.1409396.

Pinto SS, Bennett BM. 1963. Effect of arsenic triodise exposure on mortality. Arch Environ Health 7:583–591, PMID: 14058825, https://doi.org/10.1080/00039896.1963.10663587.

Rahman S, Housein Z, Dabrowska A, Mayán MD, Boobis AR, Hajji N. 2015. E2F1-mediated *FOS* induction in arsenic trioxide-induced cellular transformation: effects of global H3K9 hypoacetylation and promoter-specific hyperacetylation *in vitro*. Environ Health Perspect 123(5):484–492, PMID: 25574600, https://doi.org/10.1289/ehp.1408302.

Roboz GJ, Dias S, Lam G, Lane WJ, Soignet SL, Warrell RP Jr, et al. 2000. Arsenic trioxide induces dose- and time-dependent apoptosis of endothelium and may exert an antileukemic effect via inhibition of angiogenesis. Blood 96(4):1525–1530, PMID: 10942401.

Rodríguez-Lado L, Sun G, Berg M, Zhang Q, Xue H, Zheng Q, et al. 2013. Groundwater arsenic contamination throughout China. Science 341(6148):866–868, PMID: 23970694, https://doi.org/10.1126/science.1237484.

Rose AH, Huang Z, Mafnas C, Hara JH, Hoffmann FW, Hashimoto AS, et al. 2015. Calpain-2 inhibitor therapy reduces murine colitis and colitis-associated cancer. Inflamm Bowel Dis 21(9):2005–2015, PMID: 26076056, https://doi.org/10.1097/MIB.0000000000000471.

Schneider CA, Rasband WS, Eliceiri KW. 2012. NIH image to ImageJ: 25 years of image analysis. Nat Methods 9(7): 671–675, PMID: 22930834, https://doi.org/10.1038/nmeth.2089.

Seltenrich N. 2018. Arsenic and diabetes: assessing risk at low-to-moderate exposures. Environ Health Perspect 126(4):044002, PMID: 29634183, https://doi.org/10.1289/EHP3257.

Shen S, Li XF, Cullen WR, Weinfeld M, Le XC. 2013. Arsenic binding to proteins. Chem Rev 113(10):7769–7792, PMID: 23808632, https://doi.org/10.1021/cr300015c.

Simeonova PP, Luster MI. 2004. Arsenic and atherosclerosis. Toxicol Appl Pharmacol 198(3):444–449, PMID: 15276425, https://doi.org/10.1016/j.taap.2003.10.018.

Smedley PL, Kinniburgh DG. 2002. A review of the source, behaviour and distribution of arsenic in natural waters. Appl Geochem 17(5):517–568, https://doi.org/10.1016/S0883-2927(02)00018-5.

Spratlen MJ, Grau-Perez M, Umans JG, Yracheta J, Best LG, Francesconi K, et al. 2018. Arsenic, one carbon metabolism and diabetes-related outcomes in the Strong Heart Family Study. Environ Int 121(Pt 1):728–740, PMID: 30321848, https://doi.org/10.1016/j.envint.2018.09.048.

Storr SJ, Carragher NO, Frame MC, Parr T, Martin SG. 2011. The calpain system and cancer. Nat Rev Cancer 11(5):364–374, PMID: 21508973, https://doi.org/10.1038/nrc3050.

Vahidnia A, van der Straaten RJ, Romijn F, van Pelt J, van der Voet GB, de Wolff FA. 2008. Mechanism of arsenic-induced neurotoxicity may be explained through cleavage of p35 to p25 by calpain. Toxicol In Vitro 22(3):682–687, PMID: 18242949, https://doi.org/10.1016/j.tiv.2007.12.010.

Ye J, Coulouris G, Zaretskaya I, Cutcutache I, Rozen S, Madden TL. 2012. Primer-BLAST: a tool to design target-specific primers for polymerase chain reaction. BMC Bioinformatics 13:134, PMID: 22708584, https://doi.org/10.1186/1471-2105-13-134.